

# Spectral fluctuations in the interacting boson model <sup>\*</sup>

Yu-Qing Wu<sup>1</sup> Wei Teng<sup>1</sup> Xiao-Jie Hou<sup>1</sup> Gui-Xiu Na<sup>1</sup> Yu Zhang<sup>1;1)</sup>

Bing-Cheng He<sup>2</sup> Yan-An Luo<sup>2</sup>

<sup>1</sup> Department of Physics, Liaoning Normal University, Dalian, 116029, China

<sup>2</sup> School of Physics, Nankai University, Tianjin 300071, China

**Abstract:** The energy dependence of the spectral fluctuations in the interacting boson model (IBM) and its connections to the mean-field structures have been analyzed through adopting two statistical measures, the nearest neighbor level spacing distribution  $P(S)$  measuring the chaoticity (regularity) in energy spectra and the  $\Delta_3(L)$  statistics of Dyson and Metha measuring the spectral rigidity. Specifically, the statistical results as functions of the energy cutoff have been worked out for different dynamical situations including the U(5)-SU(3) and SU(3)-O(6) transitions as well as those near the AW arc of regularity. It is found that most of the changes in spectral fluctuations are triggered near the stationary points of the classical potential especially for the cases in the deformed region of the IBM phase diagram. The results thus justify the stationary point effects from the point of view of statistics. In addition, the approximate degeneracies in the  $2^+$  spectrum on the AW arc is also revealed from the statistical calculations.

## 1 Introduction

The interacting boson model (IBM) [1], in addition to being the important model for heavy and intermediate-heavy nuclei, also provides a theoretical laboratory for studying different many-body problems such as quantum phase transition [2–4] and quantum chaos [5–10]. The IBM has three dynamical symmetries (DSs), including U(5), O(6) and SU(3). In each dynamical symmetry limit, the system is completely integrable and corresponds to a fully regular spectrum. Away from the symmetry limits, the systems are expected to generate chaotic spectra except for the cases of mixing only the U(5) and O(6) DSs, in which the spectra are found to be still regular due to the O(5) sub-symmetry. Here, a chaotic spectrum means that the level distributions approximately obey the statistics predicted by the gaussian orthogonal ensemble (GOE) of random matrices, while a regular spectrum may approximately follow the Poisson statistics [10]. An important signature of chaos is just the statistical fluctuations of energy spectra, which is the main topic of this work.

The regular and chaotic behaviors in the context of the IBM have been extensively studied [5–11] using different theoretical tools including the energy spectral statistics [12, 13]. The chaotic map of the IBM triangle, which covers various situations in the IBM in terms of two control parameters, was revealed by Whelan and Alhassid. In particular, a nearly regular arc connecting the U(5) and SU(3) DSs has been discovered by them [8, 10] thus with the name Alhassid-Whelan arc of regularity (AW arc) given to it. A fascinating point of this arc is that its parameter trajectory may point to a very chaotic

situation with the Hamiltonian mixing the U(5), O(6) and SU(3) dynamical symmetries. However, the statistical analysis [8, 10] indicate that the spectra associated with the entire AW arc are unexpected regular (especially in a large  $N$  case [14]) in contrast to its adjacent parameter area. The AW arc has been extensively studied from different angles [15–22]. Its regularity nature has been explained in different ways including the SU(3) quasidynamical symmetry [21, 22] but remains to be clarified. In addition, the empirical signatures of this arc were also identified [17].

Most of the statistical calculations in the IBM were performed on all the excited states for a given spin. However, it is known that the spectral properties in a system may change as a function of the excitation energy. In particular, the excited state quantum phase transitions phenomena [23–28] were found to widely occur in the IBM and suggested to be connected to the stationary points of the potential functions [23, 24]. It means that the excited states in an IBM system can be divided into different “families” according to the stationary points [28]. The recent analysis [29] has revealed that the spectral fluctuations in the different “families” are indeed different especially in the chaotic region of the IBM. Such a finding was gained from the statistical calculations by predividing the excited states into different groups based on the mean-field analysis [29]. It is remained to answer whether or not the statistical results themselves can be taken as a criterion of distinguishing the excited states. In fact, an analysis of the energy dependence of the spectral fluctuations has already been given in [14] but the study focuses on the cases in the vicinity of the AW arc with only the states of zero spin being discussed. In

<sup>\*</sup> Supported by National Natural Science Foundation of China (11875158, 11875171)

1) E-mail: dlzhangyu-physics@163.com

this work, we hope to give a more general examination of the energy dependence of spectral fluctuations in the IBM to reveal the possible connections between spectral fluctuations and mean-field structures.

The investigations in this work will be placed on the cases associated with the U(5)-SU(3) and SU(3)-O(6) transitions as well as the AW arc, therefore covering most of the interesting situations in the IBM from the point of view of spectral statistics. Particularly, both zero- and nonzero-spin states will be involved in the statistical analysis. Two statistical measures, the nearest neighbor level spacing  $P(S)$  [12] and the  $\Delta_3$  statistics of Dyson and Mehta [13], will be adopted to analyze spectral fluctuation because they were successfully applied to reveal the quantal chaos and regularity in the IBM [8, 10, 14, 30, 31]. To discuss the energy dependence of spectral fluctuation, the number of statistical samples should be large enough in order to guarantee the reasonability of the statistical results evolving as a function of the excitation energy. A large- $N$  calculation of the IBM by the IBAR code [32] makes it possible to do such a kind of analysis.

The article is organized as follows. In Sec. II, the model Hamiltonian and its mean-field structure are introduced, and two statistical schemes for spectral fluctuation are described in detailed. In Sec. III, the energy dependence of the statistical results are analyzed. A summary is given in Sec. IV.

## 2 Model and statistical method

### 2.1 The Hamiltonian and mean-field structure

A Hamiltonian in the IBM framework is constructed from two kinds of boson operators:  $s$ -boson with  $J^\pi = 0^+$  and  $d$ -boson with  $J^\pi = 2^+$  [1]. To discuss different situations in the IBM, it is convenient to adopt the consistent- $Q$  Hamiltonian [33], which can be written as

$$\hat{H}(\eta, \chi) = \varepsilon \left[ (1-\eta)\hat{n}_d - \frac{\eta}{4N}\hat{Q}^x \cdot \hat{Q}^x \right]. \quad (1)$$

In the Hamiltonian,  $\hat{n}_d = d^\dagger \cdot \tilde{d}$  is the  $d$ -boson number operator,  $\hat{Q}^x = (d^\dagger s + s^\dagger \tilde{d})^{(2)} + \chi(d^\dagger \tilde{d})^{(2)}$  is the quadrupole operator,  $\eta$  and  $\chi$  are the control parameters with  $\eta \in [0, 1]$  and  $\chi \in [-\sqrt{7}/2, 0]$ , and  $\varepsilon$  is a scale factor set as 1 for convenience. The different dynamical situations in the IBM are then characterized by the different values of the control parameters  $\eta$  and  $\chi$ . Specifically, the Hamiltonian is in the U(5) DS when  $\eta = 0$ ; it is in the O(6) DS when  $\eta = 1$  and  $\chi = 0$ ; it is in the SU(3) DS when  $\eta = 1$  and  $\chi = -\frac{\sqrt{7}}{2}$ . Three DSs in the IBM describe three typical nuclear shapes including the spherical (U(5)), the axially-deformed (SU(3)) and the  $\gamma$ -unstable (O(6)).

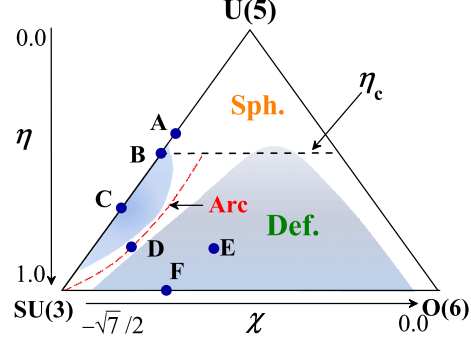


Fig. 1. The triangle phase diagram of the IBM with the dashed black line denoting the critical points of the 1st-order GSQPTs described by (4) and six parameter points A, B, C, D, E and F with  $(\eta, \chi) = (0.38, -\sqrt{7}/2)$ ,  $(0.47, -\sqrt{7}/2)$ ,  $(0.75, -\sqrt{7}/2)$ ,  $(0.88, -1.032)$ ,  $(0.88, -0.7)$  and  $(1.0, -0.9)$  being selected to analyze the spectral fluctuations in different situations. In addition, the chaotic region of the IBM identified previously [10] are schematically illustrated by two pieces of shade area with a red curve used to signify the trajectory of the AW arc of regularity passing through the chaotic region.

The mean-field structure of the IBM can be established by using the coherent state defined with [1]

$$|\beta, \gamma, N\rangle = \frac{1}{\sqrt{N!(1+\beta^2)^N}} [s^\dagger + \beta \cos \gamma d_0^\dagger + \frac{1}{\sqrt{2}} \beta \sin \gamma (d_2^\dagger + d_{-2}^\dagger)]^N |0\rangle. \quad (2)$$

The scaled potential surface corresponding to the Hamiltonian (1) in the large- $N$  limit is then given as [34]

$$\begin{aligned} V(\beta, \gamma) &= \frac{1}{N} \langle \beta, \gamma, N | \hat{H}(\eta, \chi) | \beta, \gamma, N \rangle_{N \rightarrow \infty} \\ &= (1-\eta) \frac{\beta^2}{1+\beta^2} - \frac{\eta}{4(1+\beta^2)^2} \\ &\quad \times [4\beta^2 - 4\sqrt{\frac{2}{7}} \chi \beta^3 \cos 3\gamma + \frac{2}{7} \chi^2 \beta^4]. \end{aligned} \quad (3)$$

By minimizing this potential with respect to  $\beta$  and  $\gamma$ , one can prove that the 1st-order ground state quantum phase transitions (GSQPTs) may occur at the parameter points with [34]

$$\eta_c = \frac{14}{28 + \chi^2}, \quad \chi \in [-\frac{\sqrt{7}}{2}, 0) \quad (4)$$

and the 2nd-order GSQPT takes place only at the point  $\eta_c = 1/2$  with  $\chi = 0$  on the U(5)-O(6) transitional line.

The two-dimensional phase diagram of the IBM can be mapped into a triangle. As shown in Fig. 1, each vertex of the triangle corresponds to a given DS and the

whole area is cut into two regions by the 1st-order transitional line, the spherical and deformed. It is further shown in Fig. 1 that the AW arc denoted by the dotted curve extends its trajectory from the SU(3) vertex to the interior of the triangle with the parameter trajectory being approximately described by

$$\chi = \frac{4 + (\sqrt{7} - 4)\eta}{6\eta - 8}, \quad (5)$$

which can be determined either from a minimal fraction of the chaotic phase-space volume [10] or from the minimal values of the entropy-ratio product [16]. The fraction of chaotic-space volume [10], which is defined as an phase-space integral under given conditions, is a measure of classical chaos and therefore applied to test the chaocity generated by the classical limit of the Hamiltonian. Its calculations are usually done by Monte Carlo methods. The smaller the fraction, the more regular the system is. In contrast, the entropy-ratio product, which is defined based on the Shannon information entropy of wave function [16], may be considered as a quantum measure of chaos. The wave functions and all the reference basis need to be known to calculate the entropy-ratio product. Similarly, the smaller the entropy-ratio product, the more regular the system is. In fact, the two methods agree with each other very well in characterizing the trajectory of the regular arc in the IBM (see, for example, Fig.8 in [16]), which embodies the consistency between classical and quantum chaos appearing in an IBM system. More details of the two methods can be read from [6, 10, 15, 16]. On the other hand, another approximate parametrization of the arc can be obtained as

$$\chi = \frac{2\sqrt{2} - (2\sqrt{2} + \sqrt{7})\eta}{2\eta}, \quad (6)$$

by connecting the approximate SU(3) symmetry with the AW arc of regularity [22]. One can check that Eq. (6) describes the parameter trajectory being very close to the one described by (5) for  $\eta \in [0.5, 1.0]$ .

As schematically illustrated in Fig. 1, the trajectory of the AW arc may pass through two chaotic regions in the IBM phase diagram described by the parameters  $(\eta, \chi)$  [10], while the two chaotic regions may cover most of the deformed area of the phase diagram. To analyze the spectral fluctuations in different situations, six parameter points are selected to do statistical calculations. These parameter points correspond to  $(\eta, \chi) = (0.38, -\frac{\sqrt{7}}{2}), (0.47, -\frac{\sqrt{7}}{2}), (0.75, -\frac{\sqrt{7}}{2}), (0.88, -1.032), (0.88, -0.7), \text{ and } (1.0, -0.9)$ , which have been denoted by A, B, C, D, E and F, respectively, as shown in Fig. 1. The points A, B and C are taken to illustrate three typical situations in the U(5)-SU(3) GSQPT, namely the spherical phase, critical point and

deformed phase; the points D and E are chosen to indicate the situations inside the triangle but lying on and off the AW arc; the point F represents a typical case on the SU(3)-O(6) line, which in the large- $N$  limit corresponds to a crossover [1].

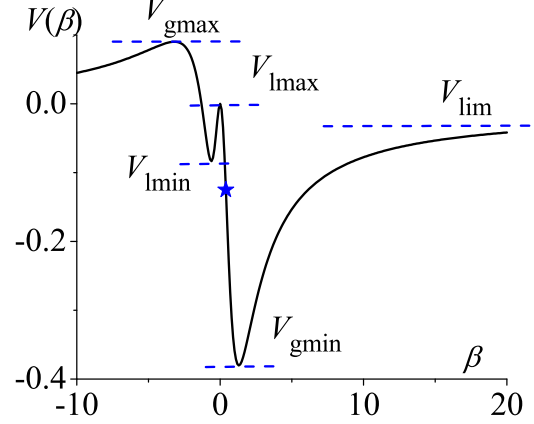


Fig. 2. The potential curve  $V(\beta)$  (in any unit) solved from (3) with  $(\eta, \chi) = (0.9, -1.3)$ . The stationary points on the curve are signified by the shot dashed lines.

One can prove that the extreme values of the potential function (3) will appear at either  $\gamma = 0^\circ$  or  $\gamma = 60^\circ$ , while the latter can be equivalently realized by taking a negative  $\beta$  value due to  $V(\beta, \gamma = 60^\circ) = V(-\beta, \gamma = 0^\circ)$ . The stationary points discussed here are defined as the extreme value points of the potential function  $V(\beta) \equiv V(\beta, \gamma = 0^\circ)$ , namely those with  $\frac{\partial V(\beta)}{\partial \beta} = 0$ . As an example, the potential curve at a typical parameter point inside the triangle is shown in Fig. 2 to illustrate stationary point structure. In general, the stationary points of a potential curve include the global minimum, the global maximum, the local minimum, the local maximum and the  $|\beta| \rightarrow \infty$  limit point, which are denoted as  $V_{gmin}$ ,  $V_{gmax}$ ,  $V_{lmin}$ ,  $V_{lmax}$  and  $V_{lim}$ , respectively, as seen in Fig. 2. Among them, the local minimal point  $V_{lmin}$  may correspond to a saddle point of  $V(\beta, \gamma)$  if observing it from the degree of freedom of  $\beta$  and  $\gamma$ . At mean-field level,  $V_{gmin}$  and  $V_{gmax}$  just correspond to the ground-state energy and highest excited energy, respectively. Therefore, more emphasis should be placed on  $V_{lmin}$ ,  $V_{lmax}$  and  $V_{lim}$ . In terms of excitation energy, the related “critical” energies are further given as

$$E_{lmin} = V_{lmin} - V_{gmin}, \quad (7)$$

$$E_{lmax} = V_{lmax} - V_{gmin}, \quad (8)$$

$$E_{lim} = V_{lim} - V_{gmin}. \quad (9)$$

It is easy to know that the energy scale in the “critical” energies is as same as the excitation energy per boson

$E/N$  (in any unit), which means that the “critical” energies defined above can be directly taken to compare the excitation energy  $E/N$  solved from the same Hamiltonian.

## 2.2 Statistical measures

To measure the spectral fluctuations in the IBM, two statistical measures will be adopted here, including the nearest neighbor level spacing distribution  $P(S)$  [12] and the  $\Delta_3$  statistics of Dyson and Mehta [13]. The spectral statistics should be performed to the so-called unfolded spectrum in order to be consistent with the requirements of the Gaussian orthogonal ensemble (GOE) [8]. First we construct the staircase function of the spectrum  $N(E)$  defined as the number of levels below  $E$  with the level energies  $E$  solved from the Hamiltonian (1).  $N(E)$  is further separated into average and fluctuating parts

$$N(E) = N_{\text{av}}(E) + N_{\text{fluct}}(E). \quad (10)$$

The average part can be expanded as a polynomial of sixth order in  $E$  [8, 14]

$$N_{\text{av}}(E) = a_0 + a_1 E + a_2 E^2 + a_3 E^3 + a_4 E^4 + a_5 E^5 + a_6 E^6 \quad (11)$$

with the expanding parameters  $a_i$  determined from the best fit to  $N(E)$ . Then, the unfolded spectrum is obtained via the mapping  $\tilde{E}_i = N_{\text{av}}(E_i)$ . With the unfolded spectrum, the nearest neighbor level spacings are obtained from

$$S_i = \tilde{E}_{i+1} - \tilde{E}_i, \quad (12)$$

and the distribution  $P(S)$  is then given as the probability of two neighboring levels to be separated by a distance  $S$ . Specifically,  $P(S)$  will be shown as the histogram of the normalized spacing and the results are further fitted to the Brody distribution [12]

$$P_\omega(S) = \alpha(1+\omega)S^\omega \exp(-\alpha S^{1+\omega}) \quad (13)$$

with  $\alpha = \Gamma[(2+\omega)/(1+\omega)]^{1+\omega}$ . The Brody distribution interpolates between Poisson statistics ( $\omega = 0$ ) characterizing a fully regular system and the Wigner distribution ( $\omega = 1$ ) indicating a completely chaotic system [8]. As a result, the intermediate value with  $\omega \in [0, 1]$  provides a quantitative estimation of the quantum chaos in the spectrum.

Spectral rigidity,  $\Delta_3(L)$ , is a measure of the deviation of the staircase function from a straight line [13]. It is defined by

$$\Delta_3(a, L) = \frac{1}{L} \min_{A, B} \int_a^{a+L} [N(\tilde{E}) - A\tilde{E} - B]^2 d\tilde{E}, \quad (14)$$

where  $A$  and  $B$  give the best local fit to  $N(\tilde{E})$  in the interval  $a \leq \tilde{E} \leq a+L$  with  $L$  being the energy length

of the interval. A rigid spectrum is supposed to give a smaller  $\Delta_3$  while a soft spectrum gives a larger  $\Delta_3$ . A smoother  $\Delta_3(L)$  can be obtained by averaging  $\Delta_3(a, L)$  over  $n_a$  intervals  $(a, a+L)$ ,

$$\Delta_3(L) = \frac{1}{n_a} \sum_a \Delta_3(a, L). \quad (15)$$

The successive intervals are taken to overlap by  $L/2$ . In the concrete calculations, a useful formula [8]

$$\begin{aligned} \Delta_3(a, L) &= \frac{n^2}{16} - \frac{1}{L^2} \left( \sum_{i=1}^n \tilde{\epsilon}_i \right)^2 + \frac{3n}{2L^2} \left( \sum_{i=1}^n \tilde{\epsilon}_i^2 \right) \\ &- \frac{3}{L^4} \left( \sum_{i=1}^n \tilde{\epsilon}_i^3 \right) + \frac{1}{L} \left( \sum_{i=1}^n (n-2i+1) \tilde{\epsilon}_i \right) \end{aligned} \quad (16)$$

with  $\tilde{\epsilon}_i = \tilde{E}_i - (a+L/2)$  is often adopted. For the Poisson statistics, it is given by

$$\Delta_3^{\text{P}}(L) = \frac{L}{15}, \quad (17)$$

while for the GOE (chaotic) case, it is approximately given by

$$\Delta_3^{\text{GOE}}(L) = \frac{1}{\pi^2} (\log L - 0.0687) \quad (18)$$

for  $L \gg 1$ . The exact form of  $\Delta_3$  statistics for the GOE and Poisson limit can be solved by the integral [8]

$$\Delta_3(L) = \frac{2}{L^4} \int_0^L (L^3 - 2L^2 r + r^3) \Sigma^2(r) dr \quad (19)$$

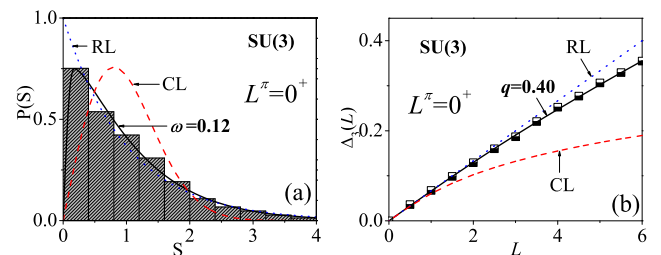
with  $\Sigma^2(L) = L$  given for the Poisson statistics and

$$\begin{aligned} \Sigma^2(L) &= \frac{2}{\pi^2} \left[ \ln(2\pi L) + \bar{\gamma} + 1 + \frac{1}{2} \left( \text{Si}(\pi L) \right)^2 \right. \\ &- \frac{\pi}{2} \text{Si}(\pi L) - \cos(2\pi L) - \text{Ci}(2\pi L) \\ &\left. + \pi^2 L \left( 1 - \frac{2}{\pi} \text{Si}(2\pi L) \right) \right] \end{aligned} \quad (20)$$

given for the GOE [8, 35]. In Eq. (20),  $\bar{\gamma}$  is the Euler constant and Si (Ci) is the sine (cosine) integral. Similar to the Brody distribution, one can fit the calculated  $\Delta_3(L)$  with the parameterization [8, 12, 14, 36]

$$\Delta_3^q(L) = \Delta_3^{\text{Poisson}}[(1-q)L] + \Delta_3^{\text{GOE}}(qL), \quad q \in [0, 1] \quad (21)$$

in order to give a quantitative estimation of the possible deviation of  $\Delta_3(L)$  from the regular ( $q = 0$ ) or chaotic limit ( $q = 1$ ).



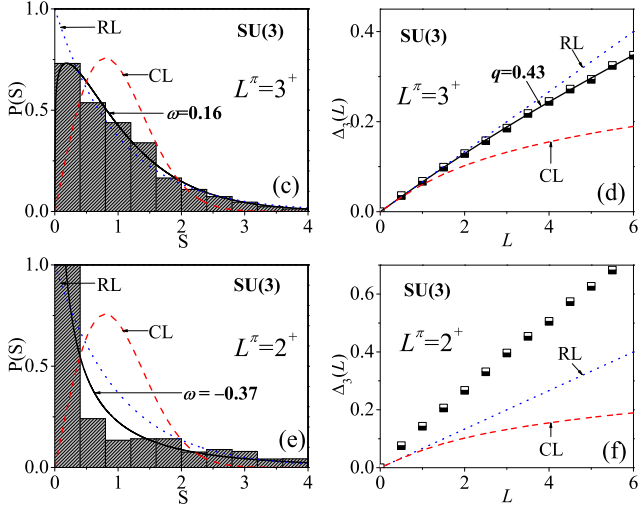


Fig. 3. (a) The  $P(S)$  statistics for the states with  $L^\pi = 0^+$  in the SU(3) limit with  $\omega$  fitted from Eq. (13) are shown to compare the regular limit (RL) and the chaotic limit (CL), which are denoted by the dotted and dashed lines, respectively; (b) The same as in (a) but for the  $\Delta_3(L)$  statistics with  $q$  fitted from Eq. (21). The panels (c)-(f) show the same statistics as in (a) or in (b) but for those with  $L^\pi = 3^+$  and  $L^\pi = 2^+$ . The calculation is performed for  $N = 200$ .

To exemplify the  $P(S)$  and  $\Delta_3$  statistics, the calculated results for the spectra with  $L^\pi = 0^+, 2^+, 3^+$  in the SU(3) limit are shown in Fig. 3. Since the SU(3) limit in the IBM corresponds to a completely integrable situation, its dynamics are expected to be close to the regular limit (the Poisson statistics). As seen in Fig. 3, the results do agree with such a expectation, giving  $\omega \sim 0.12$  ( $q \sim 0.40$ ) for the  $0^+$  spectrum and  $\omega \sim 0.16$  ( $q \sim 0.43$ ) for the  $3^+$  spectrum, which thus provides an example of regular system for reference. As for the  $2^+$  spectrum in the SU(3) limit, it is shown that the  $P(S)$  statistics indicate a negative value of  $\omega$  and the  $\Delta_3$  statistics present the values even larger than the Poisson statistics (the regular limit). This is a result of degeneracies and related to missing labels according to the analysis given in [8]. In the SU(3) limit, the missing label is the quantum number  $K$ , which usually gives two possible values  $K = 0, 2$  for the  $2^+$  states in a given SU(3) irrep  $(\lambda, \mu)$ , but this point may not affect the statistics for the  $0^+$  and  $3^+$  spectra as only one value is possible ( $K = 0$  or  $K = 2$ , respectively) for  $L^\pi = 0^+$  and  $L^\pi = 3^+$  [8]. The similar situations can also occur in the other symmetry limits or even in the cases being close to a dynamical symmetry [6, 8], where the degeneracies accordingly become the approximate ones. Since the  $q$  values fitted from Eq. (21) can not be negative and will be thus set as  $q = 0$  in the following discussions if the  $\Delta_3$  statistics is larger than

the Poisson limit like those shown in Fig. 3(f). Comparatively,  $\omega$  seems to be always a reliable indicator of the spectral fluctuations in different cases.

### 3 Evolution of the spectral fluctuations in the IBM

In this section, we will discuss the spectral fluctuations at the selected parameter points and analyze their evolutionary characters with the excitation energy. It should be mentioned that the energy-dependent quantum statistics for the large- $N$   $0^+$  spectra in the vicinity of the AW arc was previously performed in [14] with the states being divided into equal number from low energy to high energy. Here, we focus on more general situations and the states are separated according to the energy cutoff instead of equal number to do the statistical calculations. In particular, both zero and nonzero spins will be considered in the study.

As shown above, the spectral fluctuations can be measured from the fitted  $\omega$  and  $q$  values with  $\omega \in [0, 1]$  and  $q \in [0, 1]$ . In the following, both  $\omega$  and  $q$  will be given as a function of the excitation energy with each value representing the result being solved from the  $P(S)$  or  $\Delta_3(L)$  calculations for all the states below a given energy cutoff  $E/N$ . Clearly, the higher the excitation energy, the more the states involved in the statistics. It means that any changes in the statistical results with the energy cutoff just reflect the evolution of the spectral chaos with the excitation energy. To obtain a reasonable statistical result, the level numbers in the calculations at the lowest energy cutoff are required to be larger than 200. To complete the statistical analysis, we also perform the  $P(S)$  and  $\Delta_3(L)$  statistics from high energy to low energy with each value of  $\omega$  or  $q$  being solved from the statistics for all the states above a given energy cutoff. Similarly, the level numbers in the calculations at the highest energy cutoff are also required to be larger than 200. In short, the energy dependence of the spectral fluctuations will be tested from two directions, from low energy to high energy and from high energy to low energy. In the calculations, the total boson number is taken as  $N = 200$ , which means that there are totally 3434  $0^+$  states, 6767  $2^+$  states and 3333  $3^+$  states involved in the statistics calculations for each parameter point. For higher angular momentum, the number of states in the case of  $N = 200$  may increase rather rapidly, which makes the production of the states much more difficult. In consideration of the computing time, the present discussions are confined to  $L^\pi = 0^+, 2^+, 3^+$ . In the following, the selected parameter points are divided into three groups: the points A, B and C describe the U(5)-SU(3) transition, C and D characterize the situation inside the triangle but lying on and off the AW arc, respectively, and the point D represents



a typical case in the SU(3)-O(6) transition.

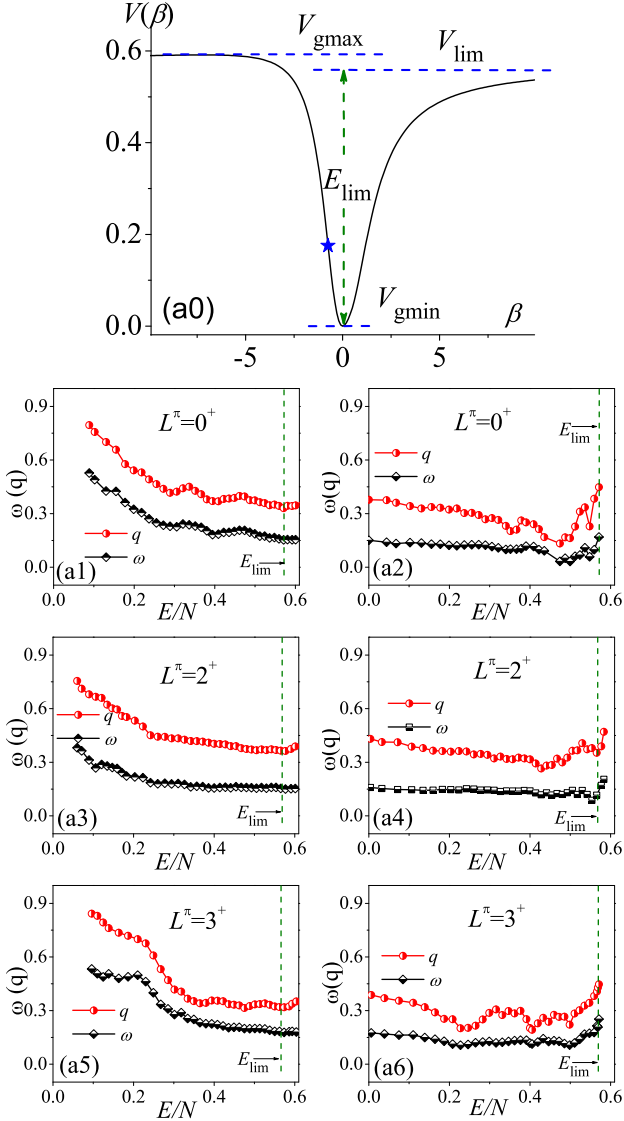


Fig. 4. The parameter point A: (a0) The potential curve  $V(\beta)$  with the blue star signifying  $\frac{\partial^2 V(\beta)}{\partial \beta^2} = 0$ ; (a1) The fitted  $\omega$  and  $q$  values evolve as functions of the per-boson energy cutoff  $E/N$  (any unit) with each  $w(q)$  value being obtained from the  $P(S)$  ( $\Delta_3(L)$ ) statistics on all the  $0^+$  levels below given  $E/N$ ; (a2) The same as in (a1) but with the statistics on the levels above given  $E/N$ . The panels (a3) and (a5) show the same results as in (a1) but for  $L^\pi = 2^+$  and  $L^\pi = 3^+$ , while (a4) and (a6) give the same results as in (a2) but for  $L^\pi = 2^+$  and  $L^\pi = 3^+$ .

### 3.1 The U(5)-SU(3) transition

The U(5)-SU(3) transition at  $\eta_c \simeq 0.47$  is proven to be a 1st-order GSQPT. The results solved from the parameter point A, B and C in this transition are shown

in Fig. 4-6, respectively. As seen in Fig. 4, the potential curve at the point A is rather simple with only one stationary point  $V_{\text{lim}}$  lying between the global minimum and maximum. It is further shown that the entire spectrum for a given spin could be rather regular if taking all the levels into the statistical calculation, which gives, for example,  $\omega \approx 0.15$  and  $q \approx 0.38$  for  $L^\pi = 0^+$ . On the other hand, the results suggest that the spectral fluctuations are not uniform in energy but the fitted  $\omega$  and  $q$  values as functions of the excitation energy are shown to be consistent with each other during the entire evolutionary process. Specifically,  $\omega$  and  $q$  for a given  $L^\pi$  may slowly decrease as functions of the energy as seen in the panels (a1), (a3) and (a5). If observing the statistics from high energy to low energy, one can find from the panels (a2), (a4) and (a6) that the  $\omega$  and  $q$  values present the nearly constant evolutions except for some small fluctuations appearing near  $E_{\text{lim}}$ . Anyway, it seems that the evolution of the spectral fluctuations in the spherical case with the simple potential configuration is relatively simple.

A similar picture can be also found in the case at the critical point (the point B) as seen from Fig. 5. It is shown that the global configuration of the potential curve at this point is as simple as the one at the point A except that two degenerate minima appear on the bottom of the potential indicating the 1st-order GSQPT. As expected, the statistical results indicate that the entire spectrum at the critical point becomes less regular compared to the spherical case. For example,  $\omega \approx 0.45$  is given in the former but  $\omega \approx 0.15$  in the latter if involving all the levels in the  $P(S)$  statistics. Similar to the spherical case, the spectral fluctuations at the critical point are not uniform in energy. One can find from (b1), (b3) and (b5) that  $\omega$  and  $q$  exhibit the consistent evolutions with the excitation energy and may reach their maximal values around  $E/N \sim 0.2$ , giving  $\omega_{\text{max}} > 0.84$  and  $q_{\text{max}} > 0.9$ , respectively. However, this feature is not easy to be illustrated from the mean-field structure as no stationary point appear nearby except the fastest changing point in  $V(\beta)$  shown around  $E/N \sim 0.15$  as seen from the panel (b0). In addition, the consistence between the  $\omega$  and  $q$  evolutions seems to be broken near  $E_{\text{lim}}$  as shown in the panels (b2) and (b6). This can be roughly explained by that the calculated  $\Delta_3(L)$  results in the related cases are already larger than the Poisson limit and thus set with  $q = 0$ . Usually, such situations only occur at  $\omega \sim 0$ .

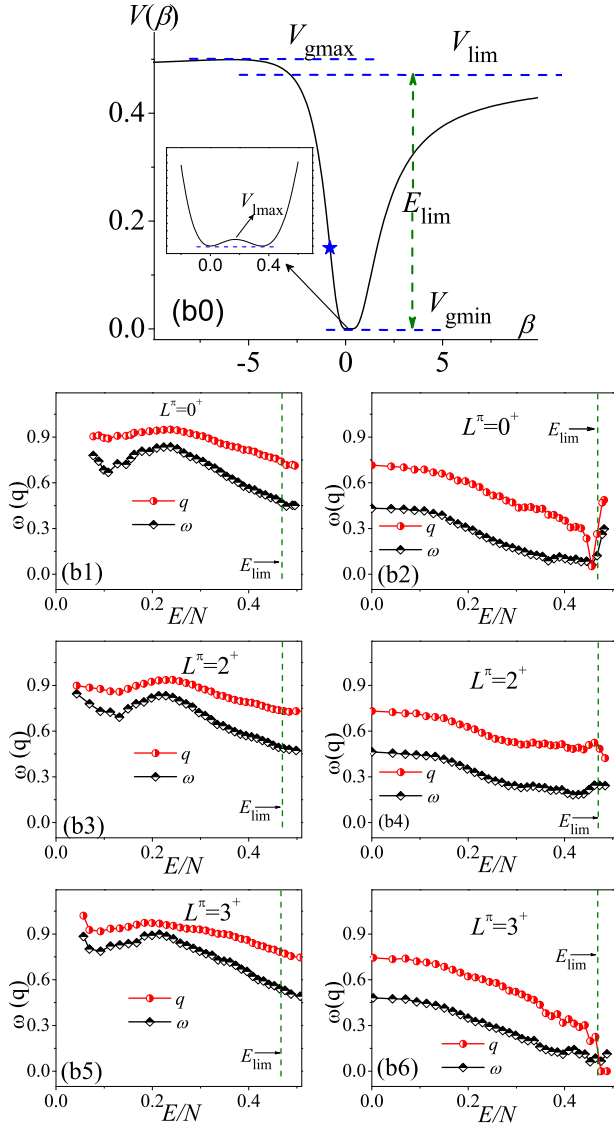


Fig. 5. The same as in Fig. 4 but for those corresponding to the parameter point B. The inset in (b0) shows an amplified picture of the potential bottom with two degenerated minimal points indicating the 1st-order GSQPT at this parameter point.

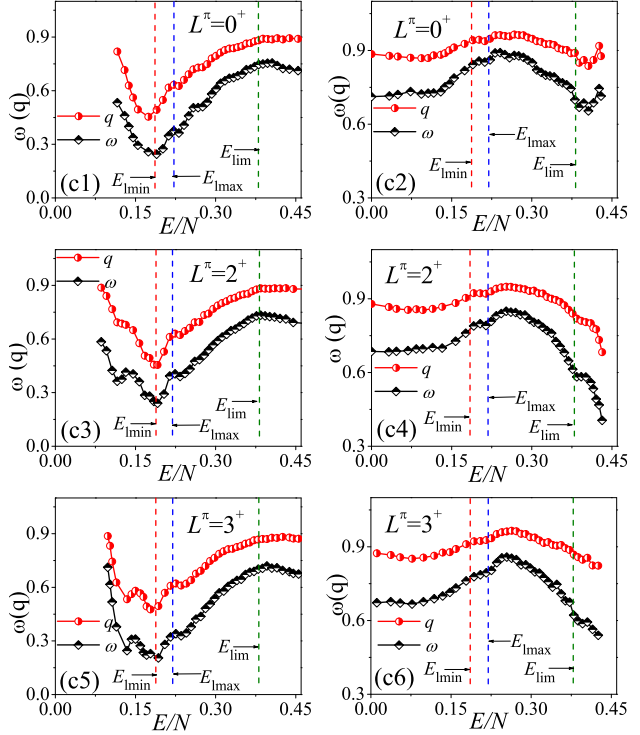
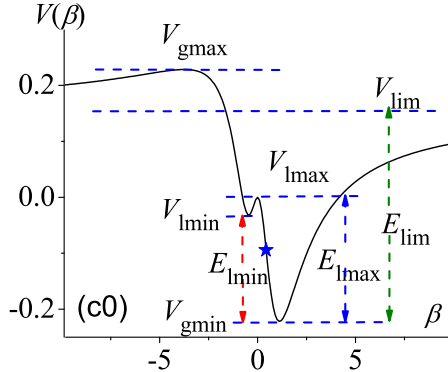


Fig. 6. The same as in Fig. 4 but for those corresponding to the parameter point C.

The more interesting case should be the one at the parameter point C because the potential  $V(\beta)$  in a deformed system can hold a richer stationary point structure. As seen from Fig. 6(c0), three stationary points  $V_{lmax}$ ,  $V_{lmin}$  and  $V_{lim}$  locate in between  $V_{gmax}$  and  $V_{gmin}$ . More importantly, the effects of these stationary points can be clearly observed in the evolutions of the statistical results as a function of the excitation energy. As shown in Fig. 6(c1), the  $\omega(q)$  values for  $L^\pi = 0^+$  present the non-monotonic evolutions with the minimal values appearing exactly at  $E_{lmin}$ , above which the influence of the stationary point can be also clearly observed near  $E_{lmax}$ . Apart from the similar evolutionary features appearing around the stationary points, the  $\omega(q)$  values for  $L^\pi = 2^+, 3^+$  meanwhile exhibit small fluctuations near  $E/N \sim 0.15$  as seen in the panels(c3) and (c5). This point to some extent reflects the effects of nonzero spins on the spectral chaos. As further seen from the panels (c2), (c4) and (c6), the influences of  $V_{lmin}$  and  $V_{lmax}$  on the spectral fluctuations have not been implicitly exhibited in the statistics from high energy to low energy but the influence of  $V_{lim}$  can be still observed. This point is not difficult to be understood since the energy levels bound above  $V_{lmax}$  in this case may occupy more than 75 percent of the total number for a given  $L^\pi$ . As a result, the influences of  $V_{lmin}$  and  $V_{lmax}$  on the spectral fluctuations may more or less be screened by the high-energy levels far from the two stationary points.

In the analysis given in [29], the stationary points  $V_{\text{Imax}}$  and  $V_{\text{Imin}}$  were taken as the phase boundaries to do the statistical analysis of the excited state quantum phase transitions (ESQPTs). Clearly, the present results further justify the reasonability of doing so. In addition, the analysis of the quantum optical models given in [37] indicate that the precursors of ESQPT phenomenon in a nonintegrable case may be accompanied by a abrupt emergence of spectral chaos. The similar situation is suggested to occur here too. Specifically, the results in Fig. 6(c1) indicate that the degree of chaoticity characterized by both  $\omega$  and  $q$  will quickly increase after  $E_{\text{Imin}}$ , which is alternatively defined as the critical energy of the ESQPT in the U(5)-SU(3) transition [28]. It is thus confirmed that the ESQPT in the nonintegrable U(5)-SU(3) cases will be also accompanied by a sudden emergence of spectral chaos.

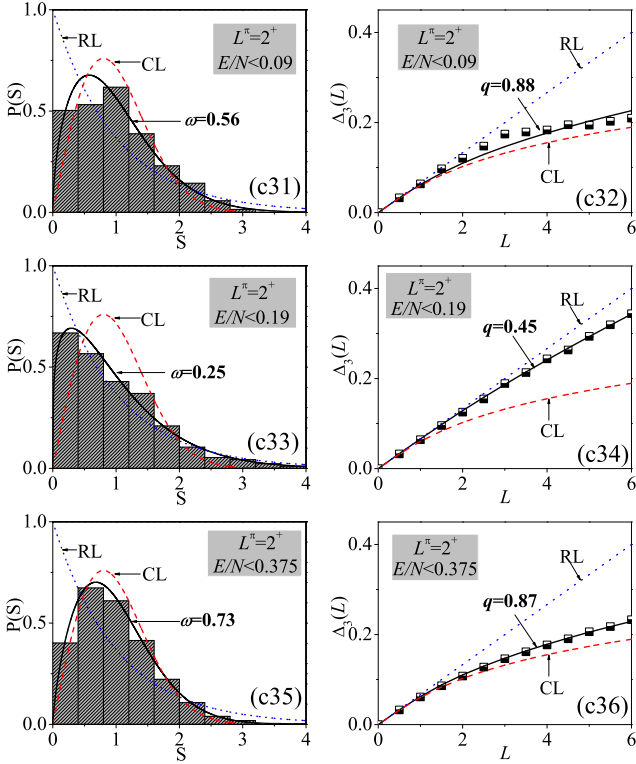


Fig. 7. The statistics for the parameter point C are shown with the statistical sample chosen as the  $2^+$  levels bound below different energy cutoffs.

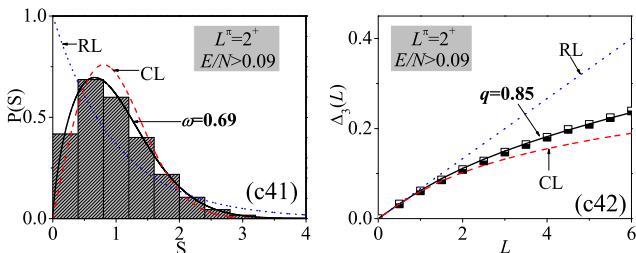


Fig. 8. The same as in Fig. 7 but taking those bound above different energy cutoffs.

To have a close look at the energy dependence of the  $P(S)$  and  $\Delta_3(L)$  statistics, we select the cases at three different energy cutoffs from the panels (c2) and (c4) of Fig 6, respectively. One can find from Fig 7 and Fig 8 that the statistical results for  $L^\pi = 2^+$  could be very different at different cutoffs. It is given by  $\omega = 0.25$  ( $q = 0.45$ ) for the spectrum below  $E/N = 0.19$  but by  $\omega = 0.79$  ( $q = 0.92$ ) for that above  $E/N = 0.19$ . Since  $E/N = 0.19$  is very close to the critical energy  $E_{\text{Imin}}$ , the results confirm again that the spectral fluctuations could be significantly different by taking the stationary point  $V_{\text{Imin}}$  as a boundary as did in [29]. In short, the spectral fluctuations in the deformed phase of the U(5)-SU(3) GSQPT are shown to be more energy dependent due to the richer stationary point structure.

### 3.2 Inside the triangle

Inside the triangle phase diagram, the parameter points D and E describe the situations on and off the AW arc, respectively. The systems on the AW arc are always expected to give regular spectra for zero [14] and nonzero spins [10]. As shown in Fig. 9, the results indicate that the entire spectrum on the AW arc is indeed very regular if involving all the levels in statistical calculations for a given  $L^\pi$ . This is highlighted by the results for  $L^\pi = 2^+$  as seen in the panels (d3) or (d4), where one can find that the statistical calculations for the entire  $2^+$  spectrum give  $\omega \sim 0$  and  $q \sim 0$ . Nonetheless, the energy dependence of the spectral fluctuations on the AW arc can be still clearly seen [14]. In particular, it is shown that the  $\omega$  and  $q$  values as a function of the excitation energy may change evidently near  $E_{\text{Imax}}$ . The results in the panel (d1) indicate that the spectral fluctuations in the  $0^+$  states will decrease until  $E_{\text{Imax}}$  and then slightly increase followed by another decrement near  $E_{\text{lim}}$ . It



means that the highest-lying states are always regular but the states near or below the stationary point  $V_{\text{lmax}}$  are also relatively regular. This picture actually agree with the classical analysis of the AW arc given in [19], where the results for the regular fraction  $f_{\text{reg}}$  (see Fig. 4 in [19]) indicate that the relative regularity of the AW arc can be to some extent enhanced near the absolute energy  $E_{\text{cl}}=0$  corresponding to the stationary point  $E_{\text{lmax}}$  discussed here.

On the other hand, the ground state and the adjacent lowest states for the AW arc should be also regular according to the analysis given in [19]. However, this point cannot be directly reflected from the  $P(S)$  and  $\Delta_3(L)$  calculations present here since the statistics require enough number of levels rather than a single ground state or a few number of lowest-lying states. As a result, the relatively larger  $\omega(q)$  values at low energy shown in the panel (d1) only imply that some relatively chaotic states may occupy a certain proportion below the corresponding energy cutoff. In fact, the results for the regular fraction given in [19] also indicate that the degree of regularity on the AW arc can be largely reduced in between the ground state energy and the absolute energy  $E_{\text{cl}}=0$ . While, such a "chaotic" character at low energy will be quickly smoothed out when involving more higher energy states in the statistical calculations. For example, if the energy cutoff is taken as the saddle point energy  $E_{\text{lmax}}$ , the degree of chaos for the  $0^+$  spectrum may decrease to  $\omega \sim 0.3$  as seen from the panel (d1).

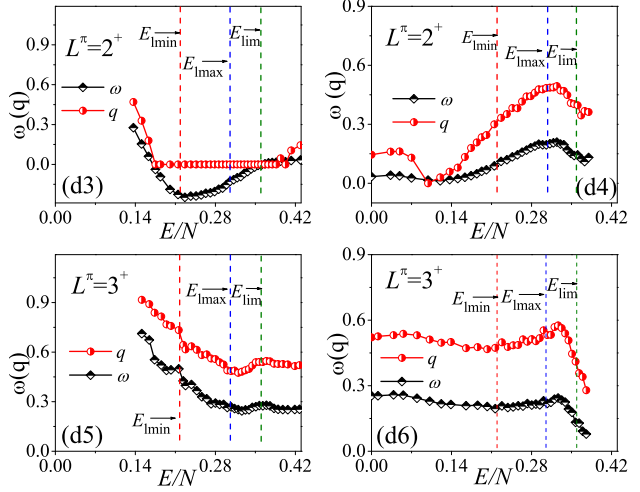
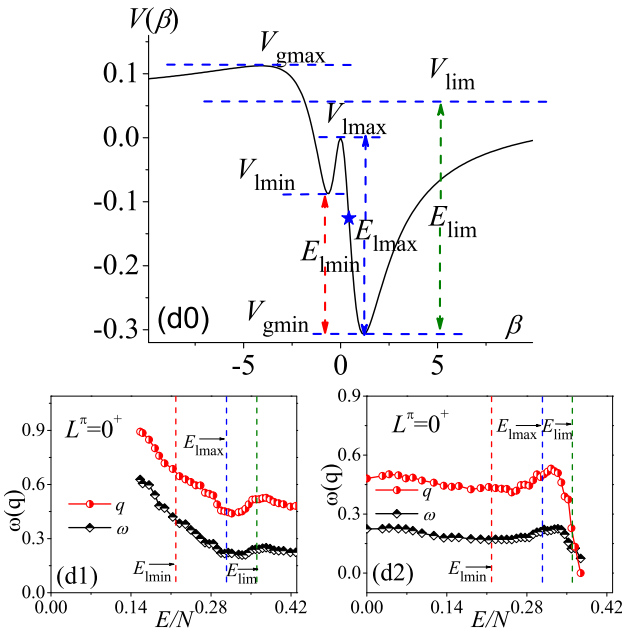


Fig. 9. The same as in Fig. 4 but those corresponding to the parameter point D (on the AW arc).

One can find from the panels (d5) and (d6) that the energy dependence of the spectral fluctuation for  $L^\pi = 3^+$  are very similar to the one for  $L^\pi = 0^+$ . In contrast, the spectral fluctuations for  $L^\pi = 2^+$  exhibit some special features. An impressive point is that  $\omega$  will become negative in the energy interval  $[E_{\text{lmin}}, E_{\text{lim}}]$  with  $q = 0$  as shown in the panel (d3). When doing the statistical calculations from high energy to low energy, the  $q = 0$  results may also appear at very low energy  $E/N \sim 0.1$  as shown in the panel (d4). According to the convention, the  $q$  values will be set by zero once the  $\Delta_3(L)$  results are larger than the Poisson limit. Similar to the case in the SU(3) symmetry discussed in Sec.IIB, the results  $\omega < 0$  and  $q = 0$  shown here may be also a result of degeneracies. It is then deduced that the degeneracies (approximate) in the  $2^+$  spectrum may be associated with the SU(3) quasidynamical symmetry [21, 22] since its parameter trajectory characterized by  $E(2_\beta^+) = E(2_\gamma^+)$  was found to be very close to the AW arc therefore suggesting a symmetry-based interpretation of the AW arc. The present results indicate that such a symmetry-based explanation of the AW arc can be tested from the point of statistics on the  $2^+$  states. However, it is not easy to point out which  $2^+$  states are approximately degenerate by directly observing their level energies in a symmetry-broken case. In addition, the validity of the underlying SU(3) quasidynamical symmetry inside was suggested to be limited to low-lying states in the large- $N$  limit [21]. So, whether or not the negative  $\omega$  values and  $q = 0$  can be fully explored by the approximate degeneracies needs to be further studied, which may be discussed elsewhere.

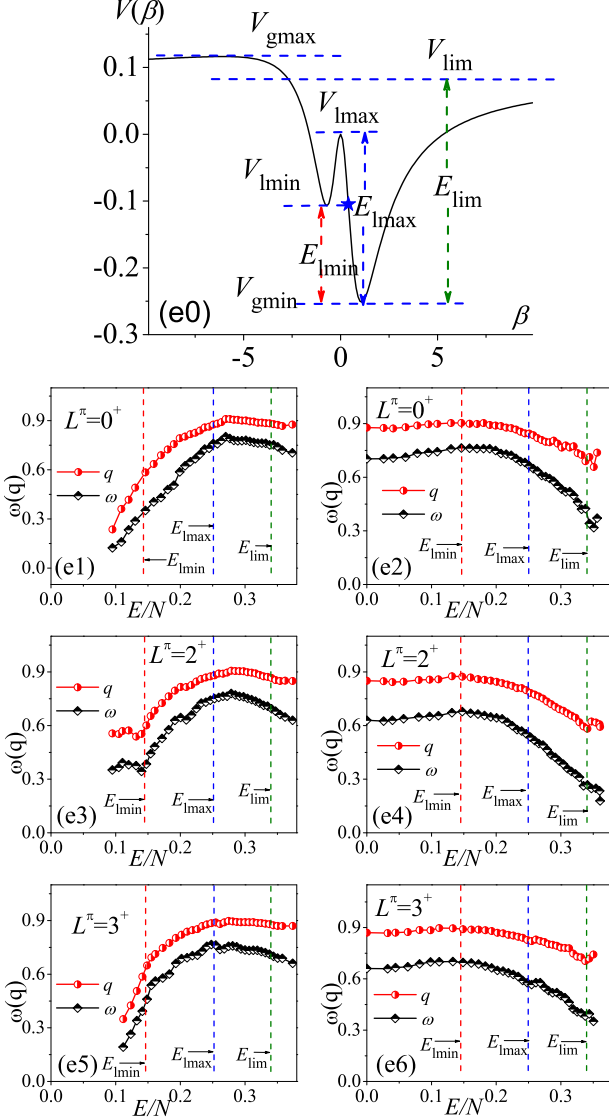


Fig. 10. The same as in Fig. 4 but for those corresponding to the parameter point E.

As for the situation off the AW arc, one can find from Fig. 10 that the potential curve at the point E is very similar to the one at the point D. Both of them have three stationary points lying in between  $V_{gmax}$  and  $V_{gmin}$ . However, the spectral fluctuations in the two cases are very different and even evolve in the opposite directions. First of all, the spectra at the point E are shown to be much more chaotic than those on the arc. For example, the  $P(S)$  statistics on all the states with  $L^\pi = 2^+$  give  $\omega \sim 0$  and  $q \sim 0$  for the point D but  $\omega > 0.6$  and  $q > 0.8$  for the point E. In addition, the results given in the panels (e1), (e3) and (e5) indicate that spectral fluctuations at the point E may increase with the excitation energy until  $E_{lmax}$  and then turn to a slow decrement. A notable point is that the  $\omega(q)$  values for  $L^\pi = 2^+$  exhibit a sudden enhancement around  $E_{lmin}$  as seen in the panel

(e3). All these features just reflect the effects of the stationary points on the spectral fluctuations at the point E. In contrast, the relatively smoother evolutions can be observed if doing the statistical calculations from high to low energy as given in the panels (e2), (e4) and (e6).

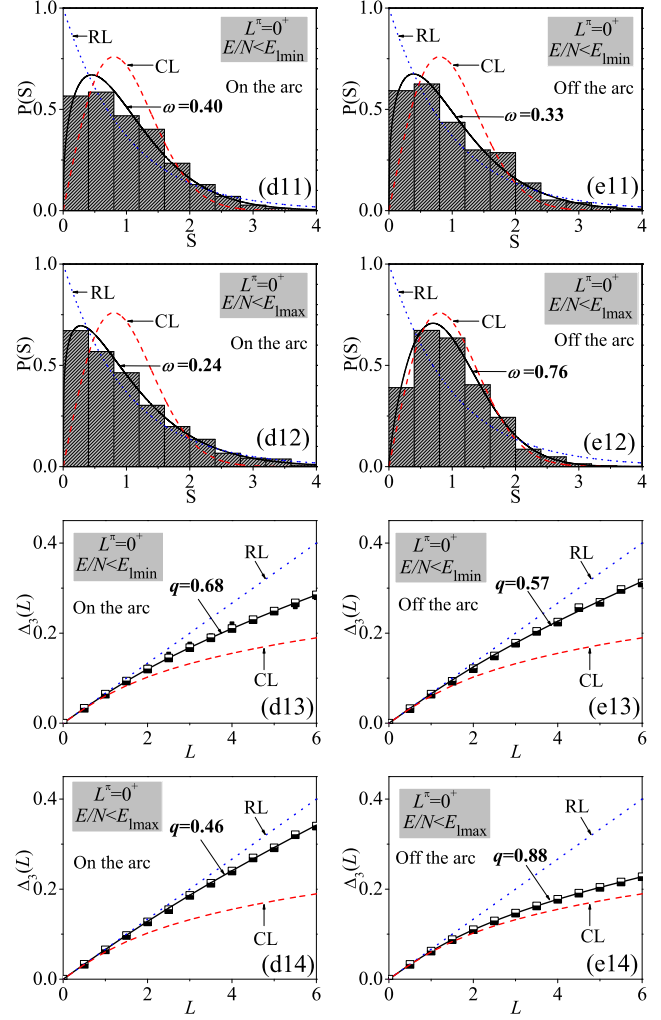
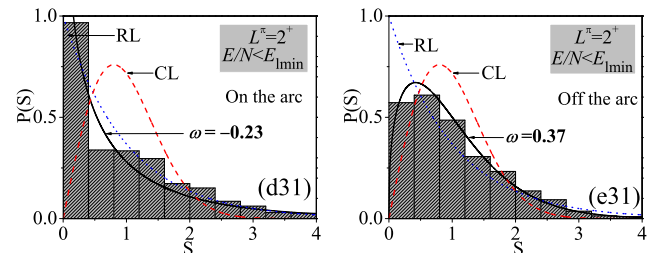


Fig. 11. To make a close comparison between the point D (on the arc) and the point E (off the arc), the statistics for the  $0^+$  levels bound below  $E_{lmin}$  and  $E_{lmax}$  in the two cases are shown.



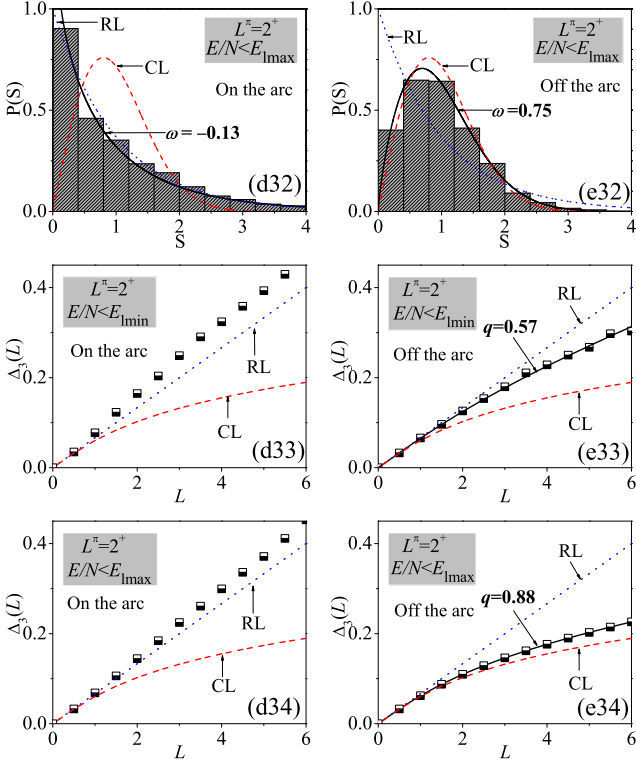


Fig. 12. The same as in Fig. 11 but for the  $2^+$  spectra.

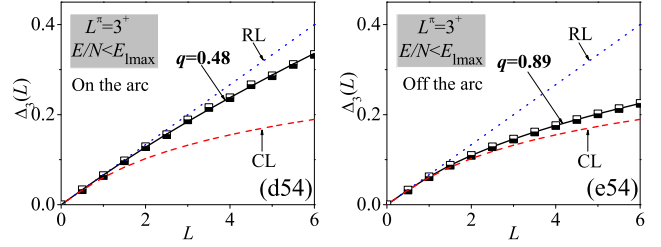
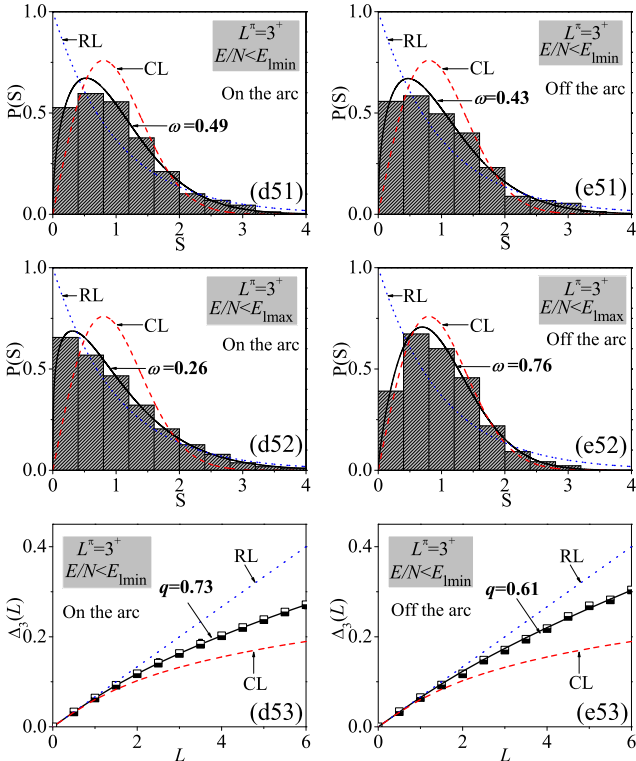
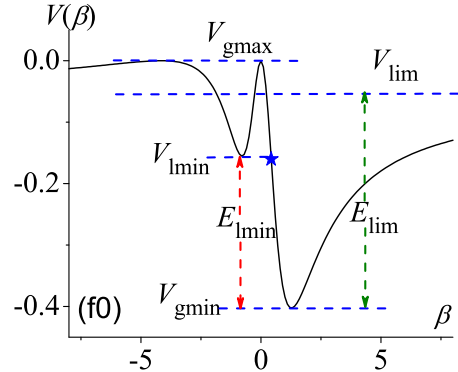


Fig. 13. The same as in Fig. 11 but for the  $3^+$  spectra.

To make a closer comparison between the cases on and off the AW arc, the concrete statistics on the levels below  $E_{lmin}$  and  $E_{lmax}$  in the two cases are extracted out from Fig. 9 and Fig. 10. As shown in Fig. 11, the results indicate that spectral fluctuations for  $L^\pi = 0^+$  below  $E_{lmin}$  have no too much difference in between two cases with  $\Delta\omega = |\omega_1 - \omega_2| = 0.07$  and  $\Delta q = |q_1 - q_2| = 0.11$ , where  $\omega(q)_{1,2}$  represent the results in the two cases. But the spectral fluctuations on the arc will dramatically decrease if more states are involved in the statistics by taking the energy cutoff  $E_{lmax}$ . Instead, the ones off the arc may become quite chaotic with  $\omega = 0.76$  and  $q = 0.88$ . Accordingly, the differences in between two cases come to the greatest with  $\Delta\omega = 0.52$  and  $\Delta q = 0.42$ , which are even larger than the results involving all the  $0^+$  levels into the statistics,  $\Delta\omega = 0.48$  and  $\Delta q = 0.40$ . This point also agree with the classical analysis of the AW arc in [19] that the relative regularity of the arc is most significant just around absolute energy  $E_{cl} = 0$  corresponding to  $E_{lmax}$ . As seen from Fig. 12, the spectral fluctuations for  $L^\pi = 2^+$  are very similar to those for  $L^\pi = 0^+$  for the case off the arc with relatively small  $\omega(q)$  at the low energy cutoff and large  $\omega(q)$  at the high energy cutoff. In contrast, the  $2^+$  spectrum on the AW arc are shown to be over regular even at the high energy cutoff with a negative  $\omega$  value, which are actually consistent with those shown in Fig. 9(d3). As shown in Fig. 13, the results for  $L^\pi = 3^+$  confirm that the regularity on the Arc will be pronounced near  $E_{lmax}$ , with the differences between the two case reaching  $\Delta\omega = 0.50$  and  $\Delta q = 0.41$  at this energy cutoff.



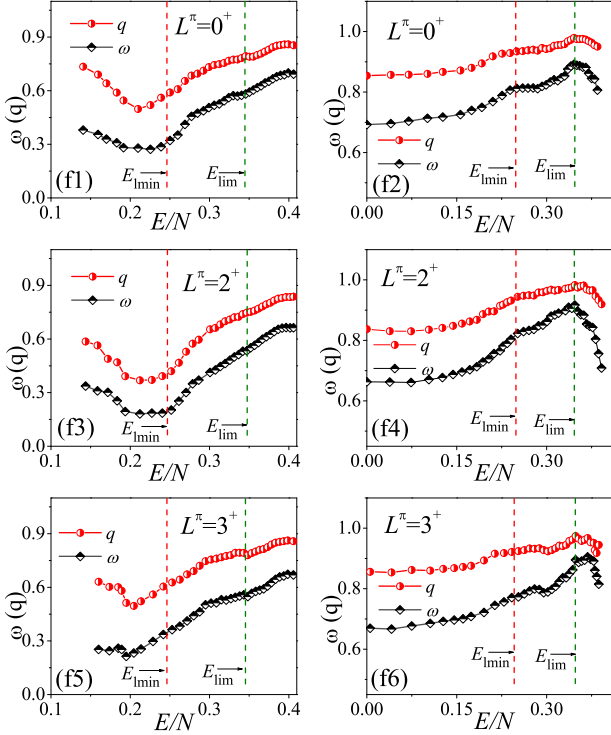


Fig. 14. The same as in Fig. 4 but for those corresponding to the parameter point F.

### 3.3 The SU(3)-O(6) transition

The parameter point F represents a typical case in the SU(3)-O(6) transition. As shown in the panel (f0), the potential curve at this point has only two stationary points lying in between  $V_{\text{gmin}}$  and  $V_{\text{gmax}}$  as its local maximal point at  $\beta = 0$  may coincide with its global maximum. The spectra for  $L^\pi = 0^+, 2^+, 3^+$  are all shown to be relatively chaotic with  $\omega > 0.6$  and  $q > 0.8$  if involving all the levels into the statistics for given spin. Like in the other cases, the spectral fluctuations in this case are not uniform in energy and the energy-dependence can be partially illustrated based on its mean-field structure. For example, the  $\omega(q)$  values as functions of the excitation energy may reach their maxima near  $E_{\text{lim}}$  as shown in the panels (f2), (f4) and (f6). Influence of  $E_{\text{lmin}}$  on spectral fluctuations can be also observed by seeing the panel

(f3), where the results imply that the spectral chaos will rapidly increase after this energy point. All these just exhibit the effects of the stationary points on the spectral fluctuations in this case.

## 4 Summary

In summary, the energy dependence of the spectral fluctuations in the IBM and its connections to the mean-field structures have been investigated for the cases across the U(5)-SU(3) GSQPT, near the AW arc and in the SU(3)-O(6) transition. Two statistical measures, the nearest neighbor level spacing distribution  $P(S)$  and the  $\Delta_3$  statistics of Dyson and Mehta, are applied to inspect the spectral fluctuations in each case. It is found that the spectral fluctuations as a function of the energy cutoff may exhibit different evolutionary behaviors in different cases but their behaviors are all shown to be closely related to the corresponding mean-field structures. Specifically, most of the sudden changes in the fluctuational evolutions can be attributed to the effects of the stationary points particularly for the cases in the deformed area of the phase diagram, where the ESQPT phenomena can be observed around the same stationary points [28]. These findings confirm again the role of the mean-field structure in understanding excited state properties. Another new finding is the appearance of negative  $\omega$  values indicating the approximate degeneracies in the  $2^+$  spectrum on the AW arc. This may provide a statistical signature of the approximate SU(3) symmetry along the AW arc [21, 22], which, however, needs to be further proved. The present large- $N$  analysis not only add new information to the chaotic map of the IBM but also offer a reference for the study of spectral fluctuations in the Bohr-Mottelson model since the model may directly link the large- $N$  limit of the IBM [1]. The discussions on spectral fluctuations can be extended to discuss the fluctuations in other quantities such as the  $B(E\lambda)$  transitions [14] or to other algebraic models including those for two-fluid systems [38–41], where the stationary point and phase structures could be much richer than the present case [38, 40]. In addition, classical measures [6] can be also applied to reveal the energy dependence of spectral fluctuations in the IBM. The related work is in progress.

## References

- 1 F. Iachello and A. Arima, *The Interacting Boson Model* (England: Cambridge University, 1987)
- 2 P. Cejnar, J. Jolie, Prog. Part. Nucl. Phys. **62**: 210-256 (2009).
- 3 P. Cejnar, J. Jolie, R. F. Casten, Rev. Mod. Phys. **82**: 2155-2212 (2010) 2155.
- 4 F. Iachello, M. A. Caprio, in *Understanding Quantum Phase Transitions*, edited by L. D. Carr (CRC, Boca Raton, FL, 2011), pp. 673-700.
- 5 Y. Alhassid, A. Novoselsky, N. Whelan, Phys. Rev. Lett. **65**: 2971-2974 (1990).
- 6 Y. Alhassid, N. Whelan, Phys. Rev. C **43**: 2637-2647 (1991).
- 7 Y. Alhassid, N. Whelan, Phys. Rev. Lett. **67**: 816-819 (1991).
- 8 Y. Alhassid, A. Novoselsky, Phys. Rev. C **45**: 1677-1687 (1992).
- 9 Y. Alhassid, N. Whelan, Phys. Rev. Lett. **70**: 572-575 (1993).
- 10 N. Whelan, Y. Alhassid, Nucl. Phys. A **556**: 42-66 (1993).
- 11 A. Leviatan, M. Macek, Phys. Lett. B **714**: 110-114 (2012).
- 12 T. A. Brody, J. Flores, J. B. French, P. A. Mello, A. Pandey, S. S. M. Wong, Rev. Mod. Phys. **53**: 385-479 (1981).
- 13 F. J. Dyson, M. L. Mehta, J. Math. Phys. **4**: 713-719 (1963).
- 14 S. Karampagia, D. Bonatsos, R. F. Casten, Phys. Rev. C **91**:

- 
- 054325 (2015).
- 15 P. Cejnar, J. Jolie, Phys. Lett. B **420**: 241-247 (1998).
  - 16 P. Cejnar, J. Jolie, Phys. Rev. E **58**: 387-399 (1998).
  - 17 J. Jolie, R. F. Casten, P. Cejnar, S. Heinze, E. A. McCutchan, N. V. Zamfir, Phys. Rev. Lett **93**: 132501 (2004).
  - 18 L. Amon, R. F. Casten, Phys. Rev. C **75**: 037301 (2007).
  - 19 M. Macek, P. Stránský, P. Cejnar, S. Heinze, J. Jolie, J. Dobeš, Phys. Rev. C **75**: 064318 (2007).
  - 20 M. Macek, J. Dobeš, P. Cejnar, Phys. Rev. C **80**: 014319 (2009).
  - 21 D. Bonatsos, E. A. McCutchan, R. F. Casten, Phys. Rev. Lett. **104**: 022502 (2010).
  - 22 D. Bonatsos, S. Karampagia, R. F. Casten, Phys. Rev. C **83**: 054313 (2011).
  - 23 M. A. Caprio, P. Cejnar, F. Iachello, Ann. Phys. **323**: 1106-1135 (2008).
  - 24 P. Cejnar, P. Stránský, M. Macek, M. Kloc, J. Phys. A **54**: 133001 (2021).
  - 25 P. Stránský, M. Macek, P. Cejnar, Ann. Phys. **345**: 73-97 (2014).
  - 26 P. Stránský, M. Macek, A. Leviatan, P. Cejnar, Ann. Phys. **356**: 57-82 (2015).
  - 27 M. Macek, P. Stránský, A. Leviatan, P. Cejnar, Phys. Rev. C **99**: 064323 (2019).
  - 28 Y. Zhang, Y. Zuo, F. Pan, J. P. Draayer, Phys. Rev. C **93**: 044302 (2016).
  - 29 W. T. Dong, Y. Zhang, B. C. He, F. Pan, Y. A. Luo, J. P. Draayer, S. Karampagia, J. Phys. G **48**: 045103 (2021).
  - 30 V. Paar, D. Vorkapić, A. E. L. Dierperink, Phys. Rev. Lett. **69**: 284-2187 (1992).
  - 31 J. Shu, Y. Ran, T. Ji, Y. X. Liu, Phys. Rev. C **67**: 044304 (2003).
  - 32 R. J. Casperson, Comput. Phys. Comm. **183**: 1029 (2012).
  - 33 D. D. Warner, R. F. Casten, Phys. Rev. C **28**: 1798-1805 (1983).
  - 34 F. Iachello, N. V. Zamfir, Phys. Rev. Lett. **92**: 212501 (2004).
  - 35 R. U. Haq, A. Pandey, O. Bohigas, Phys. Rev. Lett. **48**: 1086-1089 (1982).
  - 36 A. Hönig, D. Wintgen, Phys. Rev. A **39**: 5642-5657 (1989).
  - 37 P. Pérez-Fernández, A. Relaño, J. M. Arias, P. Cejnar, J. Dukelsky, J. E. García-Ramos, Phys. Rev. E **83**: 046208 (2011).
  - 38 J. E. García-Ramos, P. Pérez-Fernández, J. M. Arias, Phys. Rev. C **95**: 054326 (2017).
  - 39 F. Pérez-Bernal, F. Iachello, Phys. Rev. A **77**: 032115 (2008).
  - 40 M. A. Caprio, F. Iachello, Ann. Phys. **318**: 454-494 (2005).
  - 41 M. A. Caprio, J. H. Skrabacz, F. Iachello, J. Phys. A **44**: 075303 (2011).